JOURNAL OF GEOPHYSICAL RESEARCH, VOL. 102, NO. A4, PAGES 7399-7410, APRIL 1, 1997

Gravity wave seeding of equatorial plasma bubbles

Sardul Singh[1], F. S. Johnson, and R. A. Power

William B. Hanson Center for Space Sciences, Physics Program, University of Texas at Dallas, Richardson

Abstract. Some examples from the Atmosphere Explorer E data showing plasma bubble development from wavy ion density structures in the bottomside *F* layer are described. The wavy structures mostly had east-west wavelengths of 150–800 km; in one example it was about 3000 km. The ionization troughs in the wavy structures later broke up into either a multiple-bubble patch or a single bubble, depending upon whether, in the precursor wavy structure, shorter wavelengths were superimposed on the larger-scale wavelengths. In the multiple-bubble patches, intrabubble spacings varied from 55 km to 140 km. In a fully developed equatorial spread *F* case, east-west wavelengths from 690 km down to about 0.5 km were present simultaneously. The spacings between bubble patches or between bubbles in a patch appear to be determined by the wavelengths present in the precursor wave structure. In some cases, deeper bubbles developed on the western edge of a bubble patch, suggesting an east-west asymmetry. Simultaneous horizontal neutral wind measurements showed wavelike perturbations that were closely associated with perturbations in the plasma horizontal drift velocity. We argue that the wave structures observed here that served as the initial seed ion density perturbations were caused by gravity waves, strengthening the view that gravity waves seed equatorial spread *F* irregularities.

1. Introduction

Equatorial spread *F* (ESF) irregularities have been studied for over 5 decades using ionosondes, scintillations, radars, space probes (rockets and satellites), airglow, and transequatorial propagation (TEP) measurements. These irregularities do not have a uniform spatial distribution and, in general, occur instead in quasiperiodic patches [*Clemesha*, 1964; *Rottger*, 1973, 1978; *Woodman and LaHoz*, 1976; *Tsunoda et al.*, 1979; *Towle*, 1980]. *Rottger* [1973], from a TEP experiment, found median east-west spacing of ESF patches to be 380 km. The large-scale quasiperiodicity (the macroscale structure) of ESF is believed to be caused by gravity waves in the neutral atmosphere which organize the *F* region plasma into high- and low-density regions with the same horizontal wavelength as their own [*Hines*, 1960; *Whitehead*, 1971; *Beer*, 1973, 1974; *Rottger*, 1978; *Klostermeyer*, 1978; *Booker*, 1979; *Tsunoda and White*, 1981; *Kelley et al.*, 1981; *Kelley*, 1989; *Kelley and Hysell*, 1991; *Huang et al.*, 1993]. The interaction between the neutral gas and the plasma takes place, according to *Whitehead* [1971], through a mechanism called spatial resonance. According to *Beer* [1974], as a gravity wave propagates through an ionosphere with vertical ion density gradients, it causes wavelike fluctuations in ion and electron densities through collisions between neutral particles and plasma. Gravity waves also produce changes in density and temperature which affect recombination rates and hence also contribute to ion density fluctuations [*Beer*, 1973, 1974]. The gravity-wave-induced plasma perturbations thus produced are strong if the phase velocity of gravity waves and the plasma drift velocity match, which is the condition for spatial resonance. *Klostermeyer* [1978] and *Kelley* [1989] pointed out that gravity-wave-associated perturbations in the vertical component of the neutral winds generate perturbation electric fields which are alternately eastward and westward and that these fields, through $\delta E \times B$ drift, are associated with the rise of plasma in regions where the electric field is eastward and the fall in adjoining regions where the field is westward. In the presence of vertical gradients of ion density in the bottomside *F* layer, the resulting vertical displacements of the plasma produce wavelike east-west gradients in ion density. According to Klostermeyer's calculations, when the matching of velocities is perfect (perfect spatial resonance), gravity-wave-induced plasma density depletions can be as large as 1 order of magnitude. Since ion density depletions as large as 3 orders of magnitude or more have been reported in ESF structures such as satellite-detected plasma bubbles [*Hanson and Sanatani*, 1973; *McClure et al.*, 1977; *Singh*, 1989], these structures obviously cannot be produced by gravity waves alone. It has been argued [e.g., *Kelley et al.*, 1981; *Tsunoda and White*, 1981; *Kelley*, 1989; *Kelley and Hysell*, 1991; *Huang et al.*, 1993] that gravity waves possibly provide only the initial "seed" ionization perturbation and that these are then amplified by the gravitational Rayleigh-Taylor (GRT) instability [e.g., *Haerendel*, 1973; *Woodman and LaHoz*, 1976] under favorable conditions [e.g., *Mendillo et al.*, 1992].

The ground-based radar backscatter technique has clearly shown the presence of wave structure in the bottomside of the *F* layer and its close association with the development of backscatter plumes. *Tsunoda and White* [1981], using east-west scans of Altair backscatter radar, found that electron density contours in the bottomside *F* layer were altitude modulated over regions as large as 1200 km in the east-west direction with an average east-west wavelength of about 400 km, a wavelength similar to that found by *Rottger* [1973] for ESF patches. *Kelley et al.* [1981] presented Jicamarca backscatter range-time-intensity (RTI) maps that showed large vertical oscillations of the bottomside *F* layer which they ascribed to gravity waves of east-west wavelength about 680 km. *Tsunoda* [1983] also presented Altair data that showed altitude-modulated electron density contours in the bottomside *F* layer that had average east-west wavelengths of about 400 km. The upward moving lower-density regions were seen to

[1]On leave from the Physics Department, University of Ilorin, Ilorin, Nigeria.

Paper number 96JA03998.
0148-0227/97/96JA-03998$09.00

break into secondary plumes with average spacing of about 125 km. His data further showed that the west walls of depletion regions were more unstable than the east walls (east-west asymmetry). Recently, *Huang et al.* [1993] presented similar Altair data that showed nine undulations in electron density with an average east-west wavelength of about 130 km. The wave structures are believed to be caused by modulation of electron density contours by gravity waves [e.g., *Kelley*, 1989]. More evidence as to the role of gravity waves in ESF phenomenon has been provided by *Kelley et al.* [1986], *Hysell et al.* [1990], and *Kelley and Hysell* [1991]. Besides the experimental evidence, broad occurrence characteristics of ESF have been interpreted in terms of the purported role of gravity waves in triggering the phenomenon. For example, *Rottger* [1981] explained the seasonal maximum and minimum of scintillations at a given longitude in terms of the seasonal north-south movement of the intertropical convergence zone (ITCZ). According to him, gravity waves launched from thunderstorms in the ITCZ play an important role in the appearance of premidnight ESF. Similar explanation has been proffered by S. Singh et al. (Global occurrence patterns of equatorial plasma bubbles and irregularities, unpublished manuscript, 1993) for the seasonal trends of ESF at various longitudes around the globe, based on analysis of in situ data.

In this paper we present the first in situ evidence for the presence of wave structure in the bottomside of the *F* layer after sunset and the later development of plasma bubbles from the wave structure. This evidence comes from ion density and ion drift measurements from consecutive passes of the Atmosphere Explorer E (AE-E) satellite over the same longitude regions. When the AE-E was on circular orbits in the bottomside of the *F* layer, we have observed cases where the ion density along the spacecraft flight path varied in a wavelike form up to 4000 km or more in the east-west direction. East-west wavelengths ranging from 150 to 800 km were observed within the large-scale wavelike patterns in most cases. About 95 min later on the next orbit over the same longitude sector, the lower-density regions in the wave structure were seen to have burst into sharp ion density depletions or bubbles while the higher-density regions in between the lower-density regions were largely stable, thus leading to quasiperiodic bubble patches. In addition to this evidence, we have utilized simultaneous neutral wind measurements from the neutral atmosphere temperature experiment (NATE) [*Spencer et al.*, 1973] on AE-E, which clearly indicate the presence of gravity waves in the environment of the ion density wave structures, their wavelengths matching the wavelengths of ionization density structures. We have argued that gravity waves most probably cause the wavelike ion density structures that serve as seeds for the development of plasma bubbles. In section 2 we shall briefly describe the data used for the study, and in section 3 we shall present our observations, which shall then be discussed in section 4.

2. Data

This study utilized measurements from the ion drift meter (IDM) [*Hanson et al.*, 1973; *Hanson and Heelis*, 1975] on the AE-E satellite (orbital inclination 19.76°). The data used are for the period November 1976 to September 1981 when the spacecraft was in the "despun" mode (i.e., when it was three-axis stabilized) and in circular orbits. Some details of the IDM and operational characteristics of the AE-E spacecraft are available in a number of papers [e.g., *Hanson and Johnson*, 1992; *Cragin et al.*, 1985]. Briefly, the IDM had a square aperture, behind which was a four-segment collector. The instrument looked forward in the ram direction when the satellite was in the despun mode. Ion density is derived from the total current received by the four collector segments. Ratios of currents received by the upper two and the lower two segments are used to infer pitch ion-arrival angles. Similarly, ratios of currents received by the northward and southward segment pairs are used to infer yaw arrival angles. Pitch (vertical) and yaw (horizontal) components of the ion drift velocity, V_p and V_y, relative to the spacecraft are calculated by multiplying these angles in radians by the spacecraft velocity. At the altitudes concerned here, 1° in arrival angle corresponds to a velocity of about 140 m/s. The observations are presented in terms of pitch and yaw arrival angles, corrected for satellite orientation and motion relative to the Earth. An example is shown in the upper two panels in Figure 1a. Directions of the pitch and yaw velocities are indicated in these panels as up or down and north or south. Pitch and yaw measurements were made alternately, with each series of pitch measurements followed by a series of yaw measurements, each series lasting 2/3 s or 4 s corresponding to observation cycles of 4/3 or 8 s. Each series started with an offset (absolute angle) measurement which was followed by other measurements relative to the offset value at intervals of 0.03 s. The last measurement in one series and the offset value in the next series were the most nearly simultaneous measurements of the pitch and yaw angles. They are separated by 0.06 s (0.12 s) and are available every 2/3 s (4 s) when the 4/3 (8 s) cycle was operational.

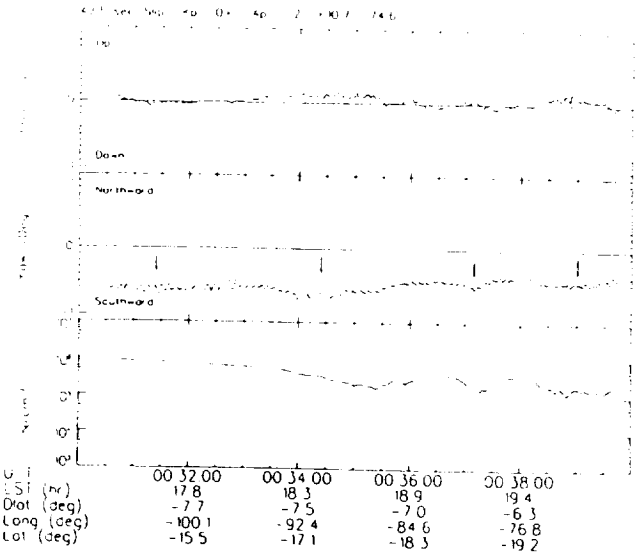

Figure 1a. Ion drift meter records from AE-E orbit 7192 at 275-km altitude. The upper two panels show pitch and yaw ion arrival angles. The bottom panel shows log ion density, which is seen to vary in a quasiperiodic manner for about 2500 km in the east-west direction beyond about 0034:00 UT. The satellite was in "slip" mode (spin axis oriented southward) with an observation cycle of 4/3 s; these are indicated at the top of the figure along with magnetic and solar activity indices. Universal time (UT), local solar time (LST), dip latitude (Dlat), geographic longitude (Long), and geographic latitude (Lat) along the spacecraft flight path are shown at the bottom.

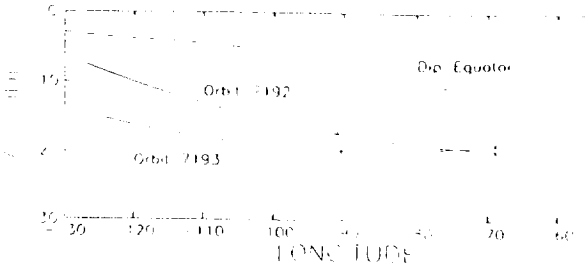

Figure 1b. The AE-E trajectories for orbits 7192 and 7193. The two successive orbits are over nearly the same latitudes, and are quite close over the longitudes of the disturbed regions, the limits of which are marked by vertical bars on the two trajectories.

These nearly simultaneous measurements were used in the computation of components of ion drift velocity parallel and perpendicular to the Earth's magnetic field, V_{perp} and V_{perp} (not shown). (These computations are valid when $B_x << B$ i.e., when the Earth's magnetic field B has only a very small component in the flight (x) direction; when B_x is not negligible by comparison with B the unknown component of horizontal drift in the x direction contributes significantly to the components of drift parallel and perpendicular to the magnetic field.) The bottom panel of Figure 1a presents measurements of ion density N_i sampled at 16 Hz by the IDM. Time, position, and dip latitude along the spacecraft flight path are shown at the bottom of the figure.

3. Observations

A visual examination of nearly 5 years of IDM data of the type discussed above revealed 19 sets of consecutive orbits over the same longitude regions. In 11 sets, clear wavy ion density structures were seen, and all but one later developed into plasma bubbles. Satellite altitude in these cases was around or below 300 km, i.e., in the bottomside F layer. In the other 8 sets, only bubbles were seen on all the consecutive orbits (the bubbles were probably preceded by wave structures which were not observed because there were no data from earlier orbits). The wave structures had east-west wavelengths ranging from 150 km to 800 km in all cases except one, in which it was about 3000 km. We present below four such cases, each involving observations from a set of consecutive orbits over the same longitudes. The data clearly show quasiperiodic ion density structures and the development of plasma bubbles from them.

3.1. Orbits 7192 and 7193

Figure 1a shows IDM records from orbit 7192 on day 77,089 (the 89th day of 1977). The satellite was at a nearly constant altitude of 275 km, i.e., in the bottomside of the F layer, and the ion density N_i along part of its flight path varied with a wavelike pattern, as seen in the bottom panel. This quasiperiodic wavy pattern extended in the east-west direction for about 2500 km, nearly 6 min of spacecraft flight time, from about 0034:00 to about 0039:45 UT. Ion density west (left) of the wavy structure was smooth at about 10^4 cm^{-3}; it is not clear if the structure extended farther east beyond 0039:45 UT, as the IDM record terminated there. The wave structure includes three ion density troughs centered around 0035:30, 0037:15, and 0039:00 UT separated by two crests; it has an average east-west wavelength of about 690 km. The wave structure was observed in the southern hemisphere between −7.5° and −6° dip latitudes in the early evening period between 18.3 and 20.0 local solar time (LST), expressed in hours and tenths. It covered longitudes between about −92° and −69°. The satellite trajectories for orbit 7192 and for the next successive orbit, 7193, over the same longitudes are shown in Figure 1b. The two passes are quite close to one another over the longitudes mentioned above.

In Figure 1a, the ion density plot in the disturbed region is kinky, with short-scale waviness, mostly in the trough regions, superimposed on the large-scale waviness of the ion density of 690 km wavelength. This is an indication that the trough regions are structured at shorter scales. Furthermore, maximum ion density in the crest regions is about 5 x 10^5 cm^{-3}, and minimum ion density in the trough regions is about 10^5 cm^{-3}. This gives a peak-to-peak change in ion density in the disturbed region of the order of a factor of 5 or less.

The pitch angle plot in the top panel of Figure 1a shows that plasma near the two crest regions is drifting downward with vertical velocities up to 13 m/s (pitch angle 0.1°), while the underdense plasma in the trough regions is moving upward with vertical velocities up to 27 m/s (pitch angle 0.2°). Plasma away from the disturbed region, between about 0031:00 and 0033:00 UT, has nearly zero drift velocity. The yaw angle plot shows that plasma in both the disturbed and undisturbed regions is drifting southward (poleward) with velocities of up to ~95 m/s. (The approximately 8-s periodicity in yaw is due to nutation of the momentum-wheel-stabilized spacecraft.) There is a progressive decrease in the southward velocity as we look to the right in the disturbed region toward later local times and closer to the dip equator. The underdense plasma near the troughs has somewhat larger southward drift velocities than the higher-density plasma in the crest regions. In the disturbed region, B_x/B was small and the V_{perp} and V_{perp} components could be calculated (they are not shown). The V_{perp} component was outward, indicating that the tubes of plasma were drifting outward in association with an

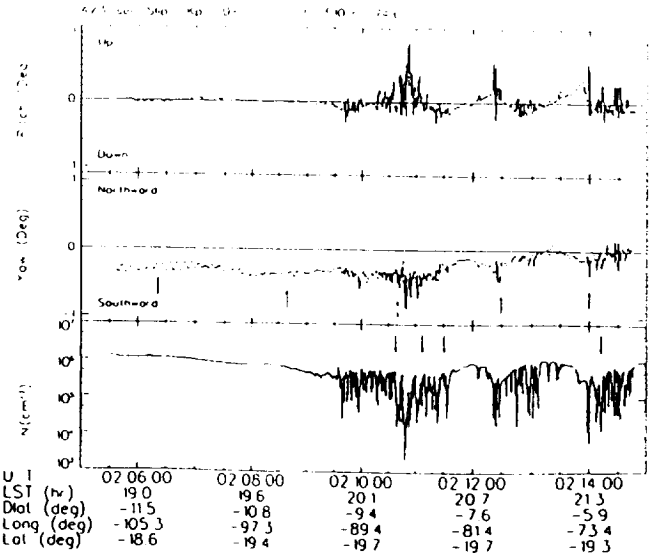

Figure 1c. Ion drift meter data for orbit 7193. The ion density troughs of Figure 1a have broken out into multiple-bubble patches.

eastward directed electric field within the tubes. The $V_{\parallel}$ component was down the field lines, indicating that plasma, at the same time, was flowing down the field lines under action of gravity.

Figure 1c shows IDM data for orbit 7193, 95 min later, at the same 275-km altitude. The figure shows three quasiperiodic bubble patches separated by comparatively undisturbed regions of higher-density plasma, over nearly the same longitudes where the wave structure of Figure 1a was seen. East-west spans of the bubble patches match well with those of the troughs of Figure 1a, suggesting their evolution from the troughs. The bubbles in all three patches are narrow and closely spaced, with average spacing of about 55 km. They have varied depths, up to 2.5 order of magnitude depletion below the ambient ion density, and have upward vertical drift velocities as large as 140 m/s and southward drift velocities up to 110 m/s. Bubbles with larger depletion levels have generally larger upward drifts. The vertical velocity of the plasma surrounding the bubbles is mostly downward, up to 30 m/s, except near 0212:30 UT. The horizontal drift velocity of the plasma surrounding the bubbles is southward, about 55 m/s in the first patch and decreasing progressively to about zero near the end of the third patch, due likely to the later local time of that patch. (Again, the effect of spacecraft nutation in producing an 8-s periodicity is prominent.) One feature of note is that in the third patch, the deepest features are on the western edge of the patch; bubble depth then decreases almost monotonically to the right. Similar east-west asymmetry in bubble depth is apparent for the portion of the first patch between 0210:45 and 0211:45 UT and also to some extent for the other part of this complex and in the second patch. Note also that ion density in the crest regions in Figure 1c is about 10^4 cm^{-3}, while in Figure 1a it was lower, about 5×10^3 cm^{-3}. This is probably to be expected since, in the 95 min between the two passes, higher-density plasma near the F layer peak and above the satellite altitude on orbit 7192 may have descended to lower height, where it was detected on orbit 7193.

Figure 1d shows an overlay of the density traces from Figures 1a and 1c, with some vertical displacement to separate the traces. A good matching of the troughs with the bubble patches clearly shows that the troughs broke out into multiple-bubble patches during the 95 min between the two passes. The higher-density crest regions remained largely free of irregularities, and the quasiperiodicity of the large-scale wave structure is still largely preserved.

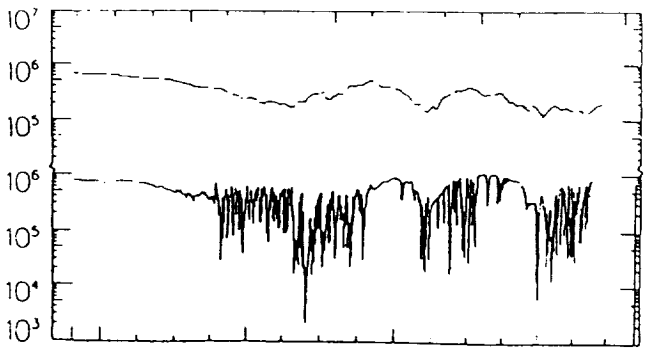

Figure 1d. A comparison of the ion density plots for orbits 7192 and 7193 with some vertical displacement to separate the plots. Ion density troughs are clearly the sites where bubble patches developed later on.

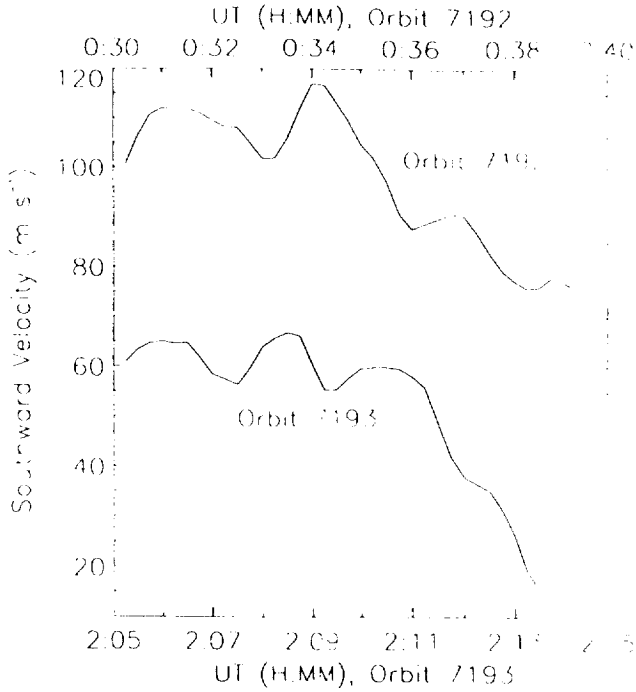

Figure 1e. Horizontal neutral wind measurements along the flight path of the AE-E spacecraft on orbits 7192 and 7193. Peaks and valleys in the wind velocity indicate the presence of gravity waves.

To examine if the wavy ion density structure in Figure 1a could be linked to gravity wave perturbations in the neutral atmosphere, we present in Figure 1e the horizontal (perpendicular to the orbital plane but largely north-south) components of neutral wind velocity measured on passes 7192 and 7193 by the NATE instrument on AE-E. The plots present 15-s averaged data from the AE-E data file (National Space Science Data Center Unified Abstract Data Files Compact Disk for Atmosphere Explorers). Measurements of components of the neutral drift could be made on AE-E in either the orbital direction or in the direction normal to the orbit plane, but not both, for any given pass. Measurements of vertical components of neutral wind velocity were made on very few passes and even these few were troubled by a malfunction in the neutral scan vane, and they were not available for any of the passes relevant to this study. Data for orbit 7192 in Figure 1e show that the winds were southward (poleward), as expected in the southern hemisphere around sunset; plasma drifts on orbit 7192, Figure 1a, were also southward. Significantly, there are wavelike perturbations in the neutral wind velocity, a clear indication of the presence of gravity waves. Four peaks in the neutral wind velocity at intervals of about 2 min are seen. They are located around 0031:20, 0034:20, 0037:10, and 0039:00 UT, with peak velocities of about 112, 117, 91, and 78 m/s, respectively. After the second peak from left, there is a large decrease in the southward wind velocity, which is most likely due to local time effect, as the poleward winds abate toward later local times after sunset. The amplitude of the periodic variation is about 10 m/s during the first half of the record, decreasing during the second half. The UT positions of the four peaks in the neutral wind velocity in Figure 1e are marked by arrows on the yaw angle plot in Figure 1a in order to compare the horizontal plasma and horizontal

wind velocities. Plasma drifts in regions near the arrows do show weak enhancements in the southward plasma drift. The peak values of the plasma drifts near the arrows are about 80, 95, 70, and 55 m/s from left to right. These values have essentially the same trend as do the peak wind velocities, for example, both drop off after the second peak. These associations between the neutral wind velocities and the plasma drift velocities suggest that the plasma drift is modulated by the gravity waves. The neutral horizontal wind velocities in the peak regions are somewhat larger than the corresponding plasma drift velocities, by a factor of about 1.3 on the average.

A further comparison of neutral and plasma drift velocities can be made for orbit 7193 from Figures 1e and 1c. In Figure 1e, the winds are still southward, but their magnitude has decreased quite drastically during the period between the two passes, from a maximum of 117 m/s on orbit 7192 to a maximum of about 68 m/s on this pass. This trend is similar to the trend of plasma drifts which decreased from a maximum of 95 m/s on orbit 7192 to 55 m/s on orbit 7193. The positions of the peak neutral wind velocities are marked on the yaw angle plot of Figure 1c. The large drop in neutral wind velocity after about 0210:40 UT seen in Figure 1e is very clearly associated with the similar drop in plasma drift velocity during that period in Figure 1c. Furthermore, the background plasma near the three arrows on the right does show larger drifts than in regions away from the arrows. The magnitudes of neutral wind velocity are again slightly larger than plasma drift velocity in the peak regions, as was the case for orbit 7192. Furthermore, the three peaks in the neutral wind velocity around 0210:40, 0212:40, and 0214:00 UT fall in the regions of the three bubble patches. A rather good association of neutral and plasma drift velocities on the two passes suggests a strong role for the neutral atmosphere in the dynamics of the F region plasma and argues that the quasiperiodic ion density structure of Figure 1a was probably caused by gravity waves through modulation of plasma drifts. We shall attempt to make such a case in the next section.

3.2. Orbits 9509, 9510, and 9511

Figure 2a shows IDM records on day 77,233 for orbit 9509 at altitude 280 km; no significant ion density variations were seen on this orbit. The pitch angle, however, oscillates weakly, the oscillations being somewhat stronger after 0540 UT. The pitch oscillations are an indication of the presence of gravity waves. On the next orbit, 9510, Figure 2b, quasiperiodic undulations in ion density are present between 180° and −153° longitude, approximately the same region where stronger pitch oscillations were observed on the earlier orbit. Wavy structure can be seen between 0715:00 and 0722:00 UT; it occurred between about 19.0 and 21.0 LT and between 12° and 9° dip latitude. The structure extends for about 3200 km, with average east-west wavelength of 540 km. There are five troughs and one bubble structure with up to about 3 orders of magnitude depletion below the ambient ion density. The bubble plasma has large vertical velocities, up to 140 m/s; the velocities are highly structured, some being downward, although these might be questioned because of the very low ion concentration. Vertical ion drifts after 0715 UT have an oscillatory trend, with plasma in the trough regions moving upward relative to the plasma in the crest regions. Unlike Figure 1a, there is very little kinkiness on the ion

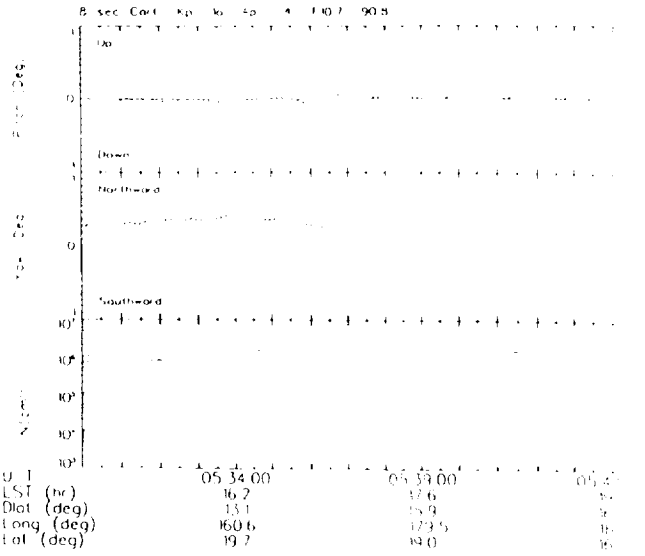

Figure 2a. Ion drift meter (IDM) data for orbit 9509 at 280 km altitude. No ion density gradients are seen, but oscillations in pitch are obvious between 0540 and 0545 UT

density plot, indicating a near-absence of shorter wavelengths superimposed on the longer wavelength of 540 km. About 95 min later on the next orbit, Figure 2c, the region of the wave structure has broken out into a series of deep, wide, and well-spaced bubbles, markedly distinct from the narrow, closely spaced bubbles in Figure 1c which evolved from the kinky troughs of Figure 1a. Three of these, between 0851:30 and 0855:30 UT, are quite active, with upward as well as some downward velocities inside them. To the left of these active bubbles, there is a broad ion density structure around 176° longitude (0850 UT). Plasma inside this structure, except the deepest part, has near-zero vertical drift velocity relative to the ambient plasma, even though there are ion density depletions as large as 2 orders of magnitude in the structure.

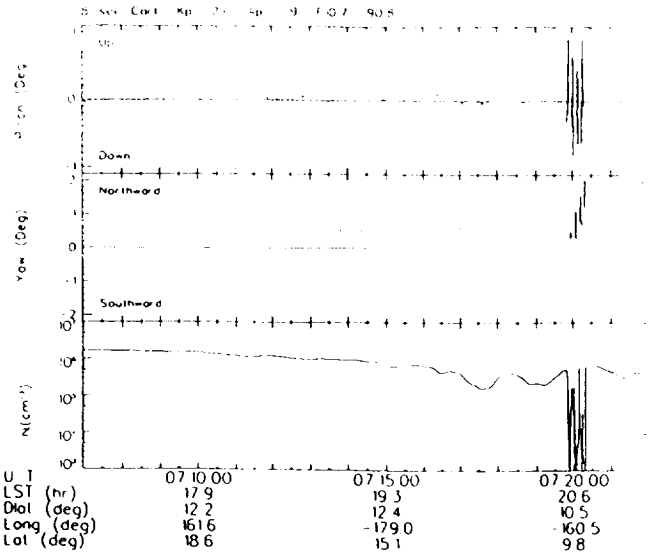

Figure 2b. Data for orbit 9510 showing a clear wavy ion density structure around the longitudes where strong oscillations in pitch were observed on earlier orbit 9509.

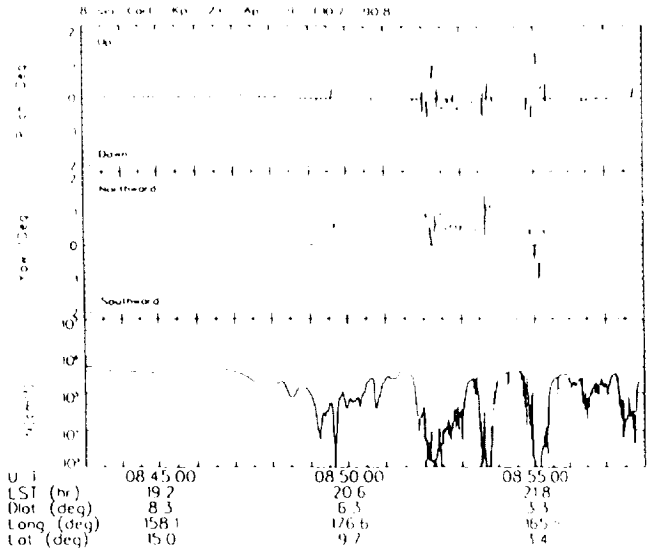

Figure 2c. Data for orbit 9511 showing bubbles that developed from the wavy ion density structure of orbit 9510.

Figure 2d shows the satellite trajectories for orbits 9510 and 9511, the latter being about 7° closer to the geographic equator between 180° and 207° (−153°) longitudes. Magnetic field lines in this region are inclined eastward relative to geographic meridians due to the nearly 10° eastward magnetic declination there. Assuming that bubbles are field-aligned vertical slabs [e.g., *Tsunoda et al.*, 1982], the satellite on orbit 9511 would enter a given eastward inclined bubble slab west of the longitude where it entered the same slab on orbit 9510, provided that the slab had no drift relative to the Earth during the time between the two orbits. However, owing to the eastward superrotation of the ionosphere as a whole during the night, the satellite may enter the same slab east of, west of, or at the same longitude as on the previous orbit, depending on the magnitude of the eastward drift. Figure 2e attempts to match the ion density plots of orbits 9510 and 9511 by visual inspection. Allowing for some eastward drift, we have assumed a small (about 3° longitude) eastward shift of the wave structure of orbit 9510 during the time between the two passes. The trough regions of the wave structure match well with bubble structures, showing quite clearly that the troughs in the wave structure broke into bubbles which are more or less single bubbles, though with some structure inside them. It is noteworthy here that the troughs of Figure 1a, by contrast, broke into several bubbles each, as seen very clearly from

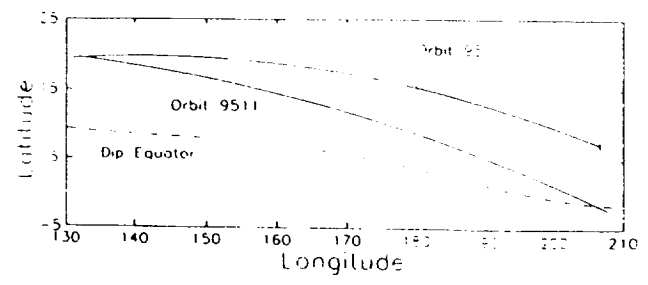

Figure 2d. Satellite trajectories for orbits 9510 and 9511. The wavy structure was between the vertical bars on the trajectory for orbit 9510.

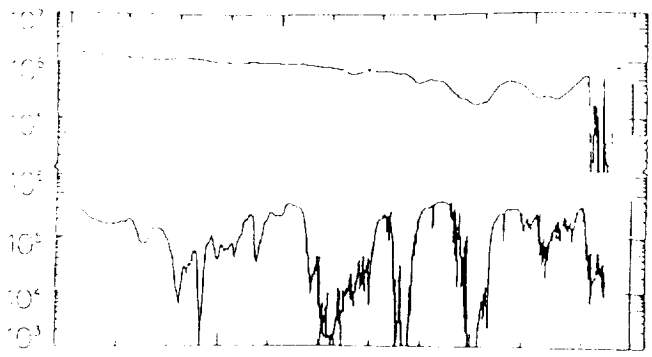

Figure 2e. A matching of the wave features of Figure 2b with the bubble features of Figure 2c.

Figure 1c. The broad ion density structure around 0850 UT on orbit 9511 appears to have developed to the west (left) of the wavy pattern of orbit 9510 during the time between the two orbits. This and the shallower troughs on the western side of the wavy structure of orbit 9510 suggest that a plasma structuring process progressed in the westward direction. Horizontal neutral wind measurements on orbits 9510 and 9511 showed perturbations in the neutral wind velocity, again indicating the presence of gravity waves in the neutral atmosphere and possibly responsible for the wavy structure of Figure 2b.

3.3. Orbits 9381, 9382, 9383, 9384, and 9385

In Figure 3a, IDM data for orbit 9381 on day 77,225 are shown; the attitude is about 282 km. The bottom panel shows small perturbations in ion density around −136° longitude (0535 UT) which are quite well associated with strong oscillations in vertical velocity (top panel), the lower ion density regions having the larger upward velocities. (The interesting pitch disturbance near 0525 UT should be ignored; it results from a commanded impulsive change in the spin angular momentum of the system.) On the following orbit, 9382, Figure 3b, an ion density trough with depletion factor

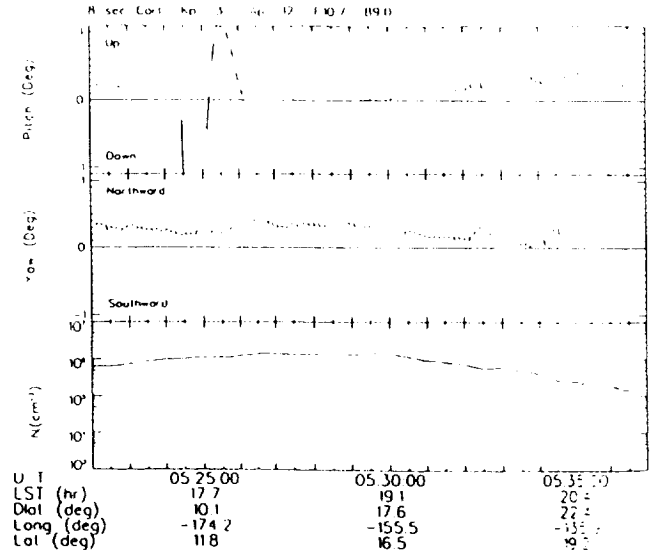

Figure 3a. Data for orbit 9381 at 282-km altitude. Small perturbations in ion density are seen near 0535 UT which have good correlation with vertical velocity in the top panel.

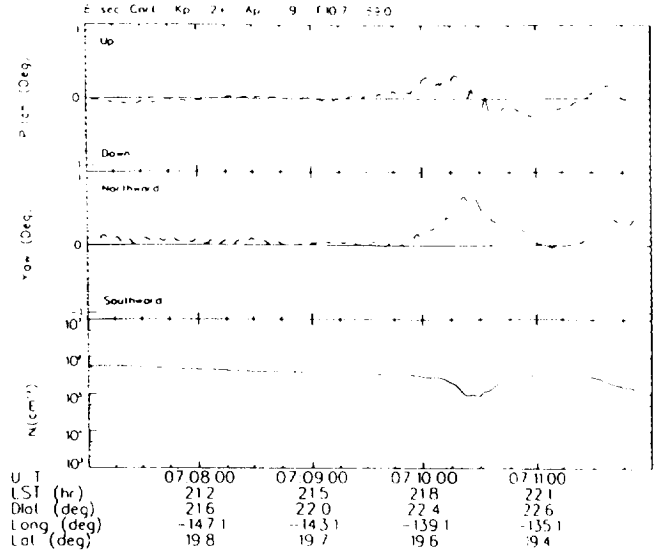

Figure 3b. Data for orbit 9382. An ion density trough is seen around the longitudes where small ion density perturbations were seen about 95 min earlier.

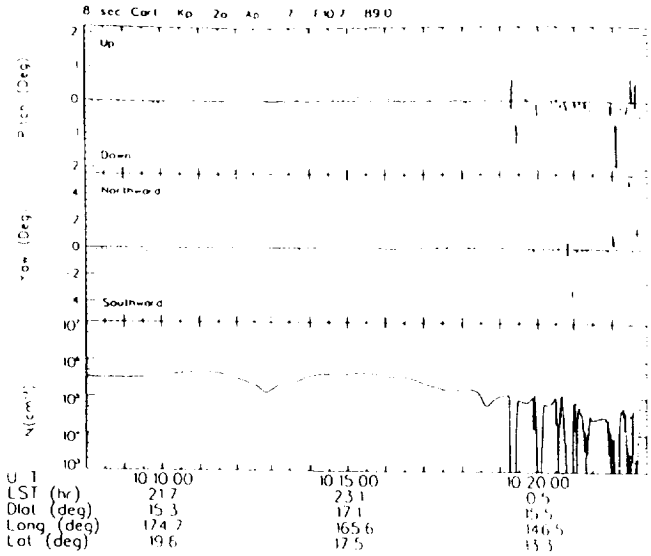

Figure 3d. IDM records for orbit 9384 showing bubbles that developed from the wave structure of orbit 9383.

up to 4 below the ambient ion density has developed around the longitude where small perturbations were observed on the previous orbit. (The abscissa scale for this plot is different from that in Figure 3a.) This level of depletion is much more than was observed on the earlier orbit 95 min earlier, indicating growth of the perturbations. Furthermore, plasma in the left half of the trough and some region farther west of it is moving upward while plasma in the right half of the trough and further to its right is moving downward, suggesting westward propagation of the gravity waves supposedly responsible for the ion density perturbations. There is also an indication of structuring of the trough region at shorter scales, as evidenced by some waviness of the density plot in the region. On the third trip of the satellite over the same longitudes (Figure 3c), a vast region extending nearly 14° west of the trough and 7° east of the trough has become well structured with four troughs interspersed with crests. The wavy structure, situated between 0842 and 0848 UT, was observed near 20° dip latitude and extends for about 2800 km with average east-west wavelength of about 690 km. Plasma in the trough regions is, curiously, moving downward relative to the surrounding plasma, while plasma west of the wavy pattern is moving upward at about 40 m/s. Substantial northward velocities are indicated for plasma in the disturbed region, with larger velocities at the trough than in other regions. Near 0845 UT, B_r/B was small, and the ion drift velocities can be resolved into $V_{\perp}$ and $V_{\parallel}$ components. In the trough region near 0846 UT, where pitch is downward and yaw is northward, $V_{\parallel}$ was outward and $V_{\perp}$ was downward along the field lines, the motion down the field lines overwhelming the outward (upward) drift. The field lines associated with the trough or incipient bubble are drifting outward. A similar situation is seen for the other troughs, but B_r/B was a little larger there. There is some structuring of the trough regions, especially of the one near 0846 UT. Furthermore, the ion density at the crests is up to 10^5 cm^{-3}, an order of magnitude lower than that in Figure 1a, due perhaps to the satellite pass now being beyond the Appleton anomaly crest (normally between about 13° and 18° dip latitudes). It is significant to note that it took

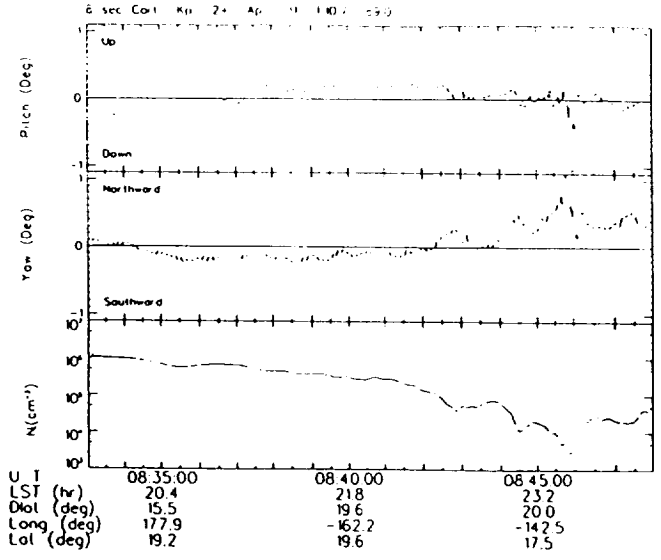

Figure 3c. IDM records for orbit 9383 showing a wavy ion density structure covering the longitudes of the trough on orbit 9382 and a vast region west and some region east of the trough.

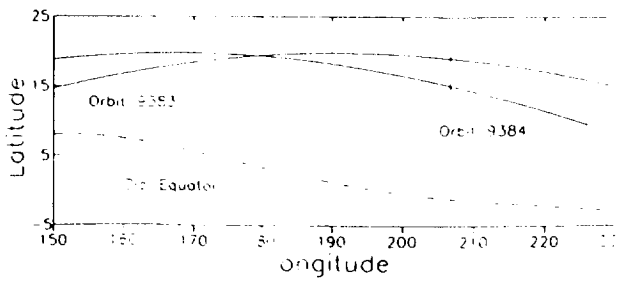

Figure 3e. The AE-E trajectories for orbits 9383 and 9384. The disturbed regions were between the vertical bars on the curves.

nearly 3 hours for the small perturbations of Figure 3a to develop into the wave structure of Figure 3c.

Figure 3d shows IDM records for orbit 9384 about 95 min later over the same longitude sector; the record ends at about −136° longitude. The spacecraft was now about 5° closer to the geographic equator than on the previous orbit when it passed over the longitudes where the wavy ion density structure of Figure 3c was detected. The wave structure has developed into about 10 sharp bubbles, some of them having about 3 orders of magnitude of depletion below the ambient density; the minimum ion density in some of them is down to about 10^2 cm^{-3} (not shown in the figure). When the ion density falls below 10^3 cm^{-3}, the IDM measurements are generally not reliable, but the ion density values in this case showed good consistency down to 10^2 cm^{-3}. Vertical ion drifts inside the bubbles are up to 300 m/s, while horizontal drifts are still larger; the drifts are both upward and downward, and northward and southward. The drift measurements in parts of the bubbles where the ion density is below about 10^3 cm^{-3} may not be reliable.

One can relate the wavy features of Figure 3c to the bubble features of Figure 3d. Figure 3e shows the trajectories of orbits 9383 and 9384. In the disturbed region, magnetic declination is about 10° E and orbit 9384 is about 5° closer to the geographic equator than 9383. Allowing for some eastward drift of the bubbles, the bubbles are likely to be seen at nearly the same longitudes where the wave structure was seen. Note that some grouping of bubbles is noticeable in Figure 3d. The trough on the extreme right, at 0846 UT in Figure 3c, appears to be associated with the group of three bubbles seen during the last 80 s of the record in Figure 3d. The middle trough, at 0844:30 UT in Figure 3c, appears to be associated with the group of bubbles between 1020:30 and 1021:20 UT in Figure 3d, and the extreme left trough near 0843 UT with the two "deep" bubbles between 1019:10 and 1020:10 UT. There are clearly some undisturbed regions between the bubble groups. Intrabubble spacing in the last two groups is about 100 km, while that between the two deep bubbles is about 270 km.

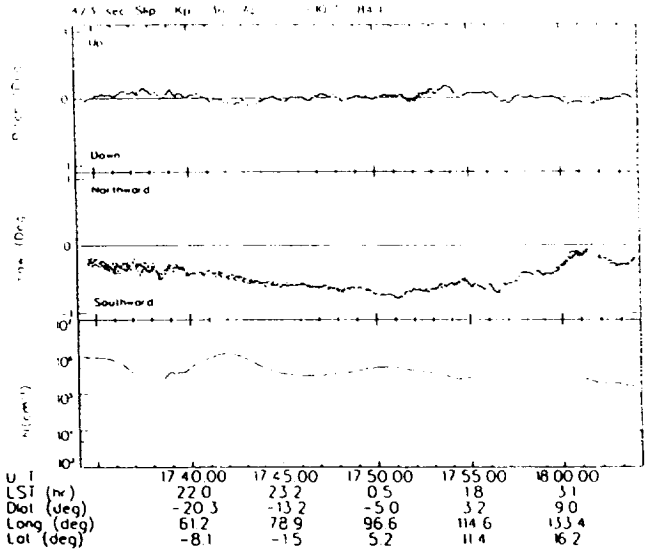

Figure 4a. IDM records for orbit 11,073 near 275-km altitude. A vast wavy ion density structure containing three troughs is seen between 1735 and 1758 UT in the bottom panel.

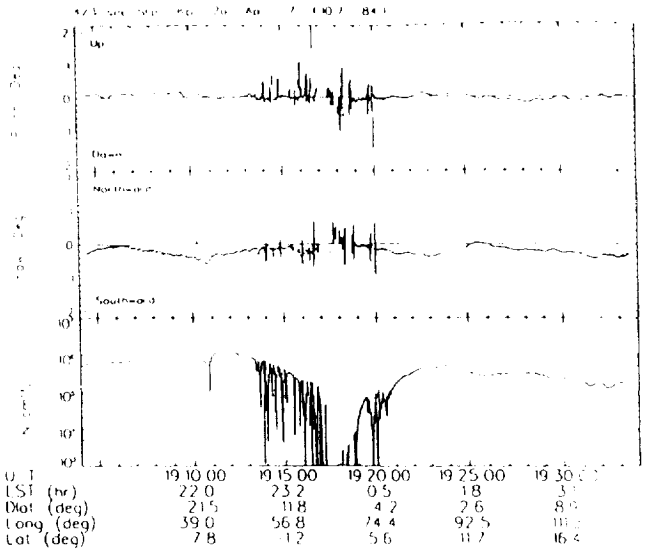

Figure 4b. Data for orbit 11,074 showing a series of bubbles that developed from the site of the first wide ion density trough of Figure 4a. Two other troughs of Figure 4a did not break out into bubbles.

IDM records on the next orbit, 9385 (not shown), showed that the bubbles decayed substantially over the next 95 min.

3.4. Orbits 11,073 and 11,074

Another example of the generation of bubbles from wavelike ion density structures in the bottomside F layer is presented in Figure 4a for day 77,330; this shows a wavelike structure with a wide, deep trough around 53° longitude (1738 UT) followed by two progressively shallower troughs to its right. The structure located between 1735 and 1758 UT is nearly 10,000 km wide with an east-west wavelength of over 3000 km. The first trough is centered around −23° dip latitude and occurred at a height of 273 km around 21.5 LT. There is kinkiness on the ion density plot in this trough region, similar to the situation in Figure 1a, which appears to be an indication that this trough region is ready to break out into smaller-scale structures. There is no kinkiness outside this trough. There are also oscillations in the vertical drift along the entire orbit. Plasma in the region of the first trough is moving upward with velocities up to 25 m/s, while that in the crest region on the right is moving downward. On the next pass, shown in Figure 4b, the first trough has broken out into a multiple-bubble patch, like the troughs of Figure 1a. The east-west width (about 3000 km) of the patch compares with the width of the trough. The patch is nearly 7° farther east of the trough position in the previous orbit; this is seen from Figure 4c which shows the trajectories of the two passes with vertical bars on them indicating the longitudes of the trough and the bubble patch. The eastward displacement corresponds to about 140 m/s eastward drift, which is not unreasonable. However, due to the small (−5°) westward magnetic declination in this region, the actual drift may be somewhat larger. Average intrabubble spacing in the region between 1913:30 and 1917:00 UT is about 140 km. The bubbles are very active, updrafting at velocities of up to 140 m/s or more. The background plasma between the bubbles is drifting downward with small velocities of about 25 m/s, typical for the nighttime [*Fejer*, 1981]. In the part of this complex between

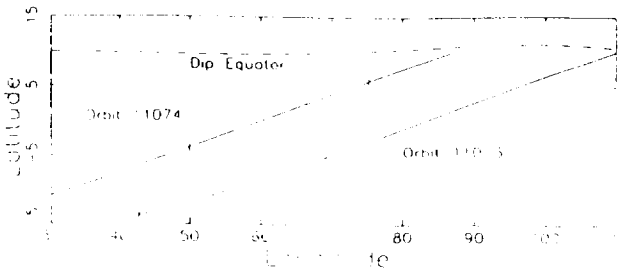

Figure 4c. Spacecraft trajectories for orbits 11,073 and 11,074. Vertical bars on the curve for orbit 11,073 indicate the longitudinal position of the first trough, while those on the curve for orbit 11,074 show the limits of the multiple-bubble patch that developed from the trough.

1917 and 1919 UT (nearly 500 km east-west) the ion density is below 10^3 cm^{-3}, and ion drift measurements are unreliable. Note that the two other shallow troughs of Figure 4a have not broken out except for two very shallow structures near 1932 UT that appear to have evolved from part of the third trough.

4. Discussion

We have presented several examples that show the presence of wavy ion density structures in the bottomside of the *F* layer. Underdense plasma in the trough regions was convecting upward, and the trough regions later broke out into bubbles. Higher-density regions between the troughs remained largely free of bubbles; these regions are believed to be not conducive to irregularity generation [e.g., *Huba et al.*, 1978; *Huba and Ossakow*, 1981; *Sperling and Goldman*, 1980]. The major question is, How might the wave structures have been produced? Figure 5 shows a possible answer to this question. In Figure 5a constant ion density contours are shown for the bottomside of the *F* layer in the absence of any disturbance. If these contours are distorted in the manner shown in Figure 5b, the AE-E spacecraft flying across them at a constant altitude records ion density along its path that varies in a nearly sinusoidal manner, as shown in Figure 5c. The distortion could result from a wavelike variation in the vertical component of plasma drift velocity, something that is indeed seen in Figure 1a. Furthermore, we saw in Figures 1a and 1c that perturbations in the horizontal component of plasma drift velocity of the background ionosphere were closely associated with perturbations in the horizontal component of the neutral wind velocity. We expect the vertical components of the neutral wind velocity also to be perturbed like the horizontal components and these perturbations to be closely associated with perturbations in the vertical components of plasma drift velocity, but data on the vertical wind component were not available. The association leads to a strong suspicion that the ion density structure was very likely caused by gravity waves propagating in the neutral atmosphere, and hence to an assertion that gravity waves probably seed plasma bubbles by providing the initial ion density perturbations that later grow into full-blown bubbles. Furthermore, we estimated the ratio of neutral wind velocity to plasma drift velocity to be about 1.3. This agrees well with a ratio of 1.2 given by *Rishbeth* [1971]. To produce a peak-to-peak ion density fluctuation of a factor of 5, as was the case in the wave structure of Figure 1a, vertical displacements of about one plasma scale height (about 15–20 km at the bottomside) are required.

Some of the wavy ion density structures seen by the AE-E extended up to 4000 km in the east-west direction. In one case the structure extended over nearly 10,000 km (Figure 4a). These spans are much larger than the spans (about 1200 km) of wave structures reported from the ground-based scanning Altair radar. The structures seen by the AE-E are more or less snapshots of the ion densities due to the very large speed (7.7 km/s) of the satellite. To be seen by the Altair radar, different parts of vast east-west structures such as the one of 10,000 km span would have to drift in the vicinity of the radar. Because the eastward drift of such structures during the nighttime due to the superrotation of the ionosphere is very small (about 100 m/s), parts of such structures would undergo considerable changes before being seen by the radar. The in situ technique therefore has an advantage over the radar technique in seeing large-scale horizontal structures as snapshots.

East-west wavelengths observed in our data varied from 150 to 800 km in all cases but one, in which it was 3000 km. An east-west wavelength as large as 3000 km has not been reported from other studies, like those from the Altair radar. The other range of wavelengths observed in this study agree well with those reported from other studies, for example, 680 km by *Kelley et al.* [1981] from Jicamarca data, 400 km by *Tsunoda and White* [1981] and 130 km by *Huang et al.* [1993] from Altair data, 380 km median spacing between ESF patches reported by *Rottger* [1973], and 350–630 km from the TAIYO satellite data by *Oya et al.* [1982].

The source of gravity waves that may have seeded the wave structures seen in this study could be in the troposphere or in

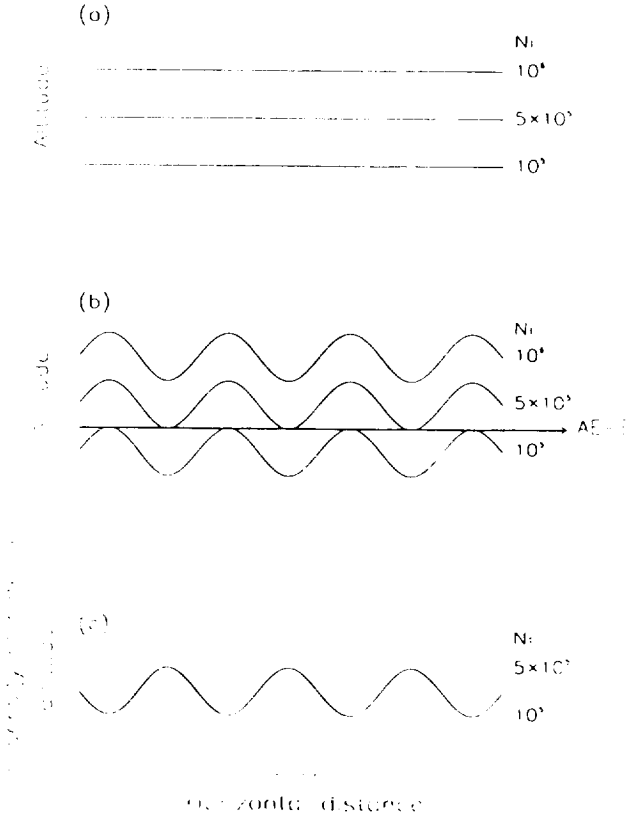

Figure 5. (a) A sketch of undisturbed ion density contours in the bottomside of the *F* layer. (b) Distorted ion density contours and the AE-E path across them at a constant altitude. (c) Quasiperiodic ion density structure recorded by the AE-E at a constant altitude as the spacecraft flew across the distorted ion density contours.

the auroral zone. *Georges* [1968] found a close relationship between the occurrence of traveling ionospheric disturbances (TIDs) of horizontal wavelengths of the order of 1000 km and magnetic storms with $K_p > 5$, the TIDs being due to gravity waves generated by atmospheric heating in the auroral zone during particle-precipitation events. *Bowman* [1978] showed a strong correlation between the onset of presunrise spread F and magnetic activity 6 hours earlier. One could therefore suspect that gravity waves originating in the auroral zone could possibly seed some of the ESF events. The wave structure of Figure 4a had a horizontal wavelength >1000 km and there was a substorm 12 hours earlier (K_p gradually increased to 5+ twelve hours earlier and then decreased), and so there might be some possibility that the gravity wave that seeded this structure originated in the auroral zone. In Figures 1, 2, and 3 the horizontal wavelengths were 500–700 km and the K_p index showed quiet magnetic conditions for 24 hours prior to the observance of the wave structures; this probably rules out the auroral zone as the source of gravity waves responsible for these structures. The gravity waves that seeded these events probably originated in the troposphere, where strong thunderstorm activity in the intertropical convergence zone is believed to be the major source of gravity waves [e.g., *Rottger*, 1981].

We now address the issue of the breakdown of larger-scale ion density structures into shorter-scale structures. We recall that strong structuring of ion density troughs was seen in some cases and not in others. In Figures 1c and 4b, the individual troughs broke into several bubbles, producing multiple-bubble patches, with average intrabubble spacing of 55 km and 140 km, respectively. In Figure 2c, by contrast, the troughs broke into wide, more or less single bubbles, though they did display some structuring inside them. The precursor wave structures in the former cases showed signs of structuring at shorter scales in the form of kinkiness of the ion density plots, which was clearly missing in the latter case. The breaking of large-scale irregularity structures into shorter-scale structures is believed to be due to a hierarchy of instabilities [*Haerendel*, 1973; *Kelly and Hysell*, 1991]. It is intriguing why the troughs break down into smaller-scale structures in some cases and not in others. Figure 6 presents high-resolution plots of ion density from the retarding potential analyzer (RPA), which was also onboard the AE-E; they show that still shorter scales are present during fully developed ESF than those seen by the IDM. The RPA in its duct mode sampled ion density at 224 Hz, corresponding to spatial resolution of about 35 m. The examples in Figure 6 show 3-s segments of RPA data beginning with UT times indicated for each segment from orbit 7193 (Figure 1c). The segments are from regions near the arrows along the ion density plot shown in Figure 1c, where bubbles were seen. The variations in ion density show quasiperiodicity at wavelengths down to about 0.5 km. Figures 1c and 6 thus clearly show that wavelengths from 690 km down to 0.5 km are simultaneously present during full-blown ESF.

In this study, plasma inside bubbles was found to move with large upward vertical and simultaneous horizontal (poleward) velocities. Vertical velocities were up to 300 m/s, and horizontal velocities had similar magnitudes. These values lie in the range given by other studies [e.g., *McClure et al.*, 1977; *Hanson and Bamgboye*, 1984; *Aggson et al.*, 1992]. In the case of Figure 1c, horizontal (poleward) and vertical (upward) velocities are up to 140 m/s. These simultaneous motions and the narrow widths of these bubbles suggest that they are like

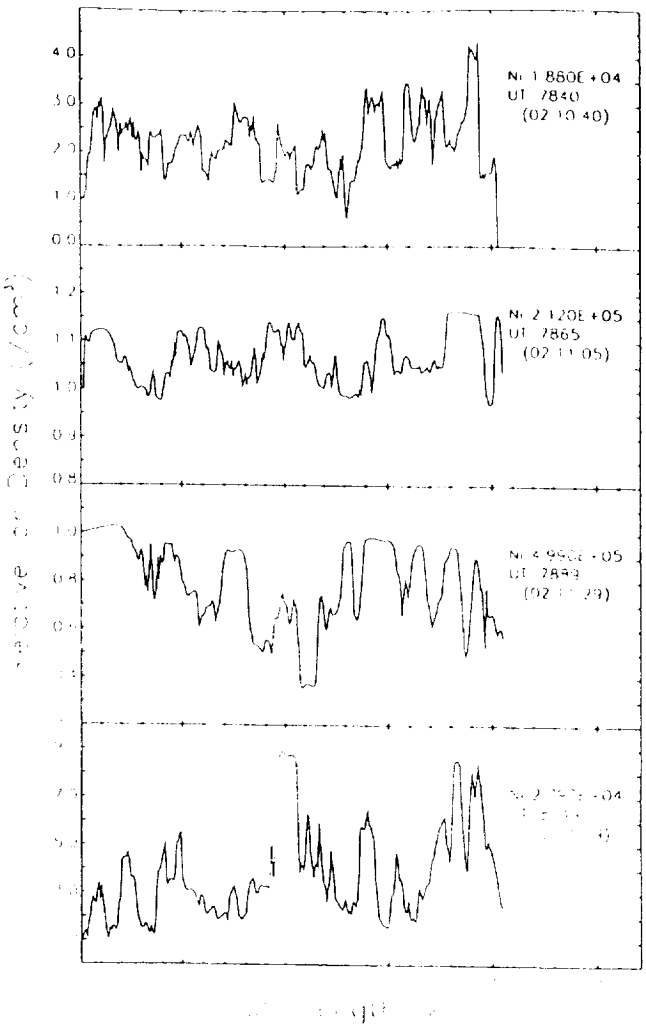

Figure 6. High-resolution 3-s segments of retarding potential analyzer data from orbit 7193 near arrows along the ion density plot in Figure 1c. The plots show variations of ion density relative to the ion density at the beginning of each plot along the flight path for 3-s periods. Ion densities and UT at the beginning of each plot are shown in each panel.

thin sheets whose north-south extents increase as they rise. Furthermore, the yaw angle plot in Figure 1c shows that the amplitude of the horizontal component of perturbation plasma drift velocity inside the deep bubble near 0210:45 UT is about 60 m/s (this is the largest ion drift velocity inside the bubble relative to the drift of the background, which is also about 60 m/s). However, the amplitude of the horizontal component of perturbation neutral wind velocity, superimposed on the background neutral wind velocity, near 0210:45 UT in Figure 1e is only about 5 m/s. We have no data on the vertical components of the neutral wind velocity for the orbits relevant to this study that could be compared with vertical plasma drift velocities. However, based on observations from the wind and temperature spectrometer (WATS) [*Spencer et al.*, 1981] on the DE 2 satellite, *Johnson et al.* [1995] haye reported that over the polar caps, the vertical components of neutral wind velocity associated with gravity waves at F region altitudes are about 3 times larger than the horizontal components. Assuming that such a relationship holds at least approximately at equatorial latitudes, the vertical neutral wind perturbation associated with gravity waves near 0210:45 UT in

Figure 1c would be about 15 m/s. The corresponding vertical plasma drift velocity, however, is about 140 m/s, as seen from the pitch plot in Figure 1c. Since the amplitude of perturbation plasma velocity cannot exceed the amplitude of perturbation neutral wind velocity due to gravity waves even for perfect spatial resonance condition [*Kelley*, 1989], it is obvious that gravity waves alone could not have produced the large perturbation plasma velocity in the bubble and that further amplification must have been produced by the GRT instability.

In Figure 1c, deeper bubbles were seen at the western edges of some of the bubble patches which evolved from ion density troughs. We note that the west walls of upwellings (in radar data), which are equivalents of ion density troughs in this study, were found by *Tsunoda* [1983] to be more unstable than the east walls, and he ascribed this east-west asymmetry in plume generation to eastward neutral winds blowing across the upwellings. His study also speculated on the possible existence of an east-west asymmetry in in situ data. The asymmetry in bubble depth seen in Figure 1c probably indicates greater instability of the western sides of the troughs than of the eastern sides and hence seems to confirm Tsunoda's observation in at least some cases. It is suggested that neutral wind measurements in conjunction with ion density measurements be carefully examined to ascertain the cause of the asymmetry.

Last, there is the question, Is ESF development inevitable whenever seed perturbations are present? *Mendillo et al.* [1992] have suggested that in addition to the presence of a seed perturbation and a postsunset rise of the *F* layer, a third factor, the absence of a strong transequatorial thermospheric wind, is a necessary condition for ESF appearance. This suggestion is in line with the hypothesis of *Maruyama and Matuura* [1984], according to which ESF activity is suppressed by strong north-south winds. More detailed studies should be directed to confirm the hypothesis. Meanwhile, gravity waves do seem to control the ESF phenomenon by the seeding mechanism, and they also seem to control the spacings between bubbles or plumes. Considering the wide spectrum of wavelengths to which the ionosphere responds via spatial resonance [*Kelley et al.*, 1981], the east-west spacings of perhaps the majority of bubbles seen by the AE-E can be satisfactorily explained.

5. Summary and Conclusions

The study has presented several pieces of evidence that show bubble development from wavy ion density structures in the bottomside of the *F* layer. The wave structures observed had east-west wavelengths of 150–800 km; in one case it was 3000 km. Ionization troughs in these structures broke out into multiple-bubble patches in some cases and into more or less single bubbles in others. In one case of full-blown ESF, wavelengths from 690 km down to 0.5 km were present simultaneously. A tendency for deeper bubbles to appear on the western edge of a multiple-bubble patch was observed in some cases. Simultaneous neutral wind measurements showed wavelike perturbations in the neutral horizontal wind velocity, indicative of the presence of gravity waves. The perturbations were further closely associated with perturbations in the horizontal components of plasma drift velocity of the background ionosphere. Gravity waves in the environment of the wavy structures probably caused the wavelike ion-density structures and hence provided the initial seed ion density perturbations. A consideration of plasma velocities inside bubbles and simultaneous neutral wind velocities suggests that gravity waves alone cannot cause the large plasma velocities inside bubbles and that a plasma instability is required for further amplification. Lack of strong magnetic disturbances prior to the development of most of the wave structures seen in this study suggests that the lower atmosphere is the more likely source of gravity waves that seed bubbles.

Acknowledgments. This work was supported by NASA grant NAGW-4002. The authors thank W. B. Hanson posthumously for providing the seminal ideas for this study and R. A. Heelis for valuable discussions.

The Editor thanks J. M. Forbes and another referee for their assistance in evaluating this paper.

References

Aggson, T. L., N. C. Maynard, W. B. Hanson, and Jack L. Saba, Electric field observations of equatorial bubbles, *J. Geophys. Res.*, *97*, 2997, 1992.

Beer, T., Spatial resonance in the ionosphere, *Planet. Space Sci.*, *21*, 297, 1973.

Beer, T., *Atmospheric Waves*, John Wiley, New York, 1974.

Booker, H. G., The role of acoustic gravity waves in the generation of spread-F and ionospheric scintillation, *J. Atmos. Terr. Phys.*, *41*, 501, 1979.

Bowman, G. G., A relationship between magnetic substorms, ionospheric height rises and the occurrence of spread F, *J. Atmos. Terr. Phys.*, *40*, 713, 1978.

Clemesha, B. R., An investigation of the irregularities in the F region associated with equatorial type spread F, *J. Atmos. Terr. Phys.*, *26*, 91, 1964.

Cragin, B. L., C. E. Valladares, W. B. Hanson, and J. P. McClure, Bottomside sinusoidal irregularities in the equatorial *F* region, 2, Cross-correlation and spectral analysis, *J. Geophys. Res.*, *90*, 1721, 1985.

Fejer, B. G., The equatorial ionospheric electric fields: A review, *J. Atmos. Terr. Phys.*, *443*, 377, 1981.

Georges, T. M., HF Doppler studies of travelling ionospheric disturbances, *J. Atmos. Terr. Phys.*, *30*, 735, 1968.

Haerendel, G., Theory of equatorial spread F, report, Max Planck Inst. für Phys. und Astrophys. Res., Garching, Germany, 1973.

Hanson, W. B., and D. K. Bamgboye, The measured motions inside equatorial plasma bubbles, *J. Geophys. Res.*, *89*, 8997, 1984.

Hanson, W. B., and R. A. Heelis, Techniques for measuring bulk gas-motions from satellites, *Space Sci. Instrum.*, *1*, 493, 1975.

Hanson, W. B., and F. S. Johnson, Lower midlatitude ionospheric disturbances and the Perkins instability, *Planet. Space Sci.*, *40*, 1615, 1992.

Hanson, W. B., and S. Sanatani, Large N_i gradients below the equatorial *F* peak, *J. Geophys. Res.*, *78*, 1167, 1973.

Hanson, W. B., D. R. Zuccaro, C. R. Lippincott, and S. Sanatani, The retarding potential analyzer on Atmosphere Explorer, *Radio Sci.*, *8*, 333, 1973.

Hines, C. O., Internal atmospheric gravity waves at ionospheric heights, *Can. J. Phys.*, *38*, 1441, 1960

Huang, C. O., M. C. Kelley, and D. L. Hysell, Nonlinear Rayleigh-Taylor instabilities, atmospheric gravity waves, and equatorial spread *F*, *J. Geophys. Res.*, *98*, 15,631, 1993.

Huba, J. D., and S. L. Ossakow, On 11-cm irregularities during equatorial spread *F*, *J. Geophys. Res.*, *86*, 829, 1981.

Huba, J. D., P. K. Chaturvedi, S. L. Ossakow, and D. M. Towle, High-frequency drift waves with wavelengths below the ion gyroradius in equatorial spread *F*, *Geophys. Res. Lett.*, *5*, 695, 1978.

Hysell, D. L., M. C. Kelley, and W. E. Swartz, Seeding and layering of equatorial spread *F* by gravity waves, *J. Geophys. Res.*, *95*, 17,253, 1990.

Johnson, F. S., W. B. Hanson, R. R. Hodges, W. R. Coley, G. R. Carignan, and N. W. Spencer, Gravity waves near 300 km over the polar caps, *J. Geophys. Res.*, *100*, 23,993, 1995.

Kelley, M. C., *The Earth's Ionosphere*, Academic, San Diego, Calif., 1989.

Kelley, M. C., and D. L. Hysell, Equatorial spread-F and neutral atmospheric turbulence: A review and a comparative anatomy, *J. Atmos. Terr. Phys.*, *53*, 695, 1991.

Kelley, M. C., M. F. Larsen, C. LaHoz, and J. P. McClure, Gravity wave initiation of equatorial spread *F*: A case study, *J. Geophys. Res.*, *86*, 9087, 1981.

Kelley, M. C., et al., The Condor equatorial spread *F* campaign: Overview of results of the large-scale measurements, *J. Geophys. Res.*, *91*, 5487, 1986.

Klostermeyer, J., Nonlinear investigation of the spatial resonance effect in the nighttime equatorial *F* region, *J. Geophys. Res.* *83*, 3753, 1978.

Maruyama, T., and N. Matuura, Longitudinal variability of annual changes in activity of equatorial spread *F* and plasma bubbles, *J. Geophys. Res.*, *89*, 10,903, 1984.

McClure, J. P., W. B. Hanson, and J. H. Hoffman, Plasma bubbles and irregularities in the equatorial ionosphere, *J. Geophys Res.*, *82*, 2650, 1977.

Mendillo, M., J. Baumgardner, X. Pi, P. J. Sultan, and R. Tsunoda, Onset conditions for equatorial spread *F*, *J. Geophys. Res.*, *97*, 13,865, 1992.

Oya, H., T. Takahashi, A. Morioka, and H. Miyaoka, Wavy patterns of ionospheric electron density profiles triggered by TID – Observation results of the electron density by TAIYO satellite, *J. Geomagn. Geoelectr.*, *34*, 509, 1982.

Rishbeth, H., Polarization fields produced by winds in the equatorial F region, *Planet. Space Sci.*, *19*, 357, 1971.

Rottger, J., Wavelike structures of large scale equatorial spread F irregularities, *J. Atmos. Terr. Phys.*, *35*, 1195, 1973.

Rottger, J., Drifting patches of equatorial spread *F* irregularities–Experimental support for the spatial resonance mechanism in the ionosphere, *J. Atmos. Terr. Phys.*, *40*, 1103, 1978.

Rottger, J., Equatorial spread-*F* by electric fields and atmospheric gravity waves generated by thunderstorms, *J. Atmos. Terr. Phys.*, *43*, 453, 1981.

Singh, S., A morphological study of satellite-detected plasma bubbles in the equatorial ionosphere, 205 pp., Ph. D. thesis, Univ. of Ilorin, Ilorin, Nigeria, 1989.

Spencer, N. W., H. B. Niemann, and G. R. Carignan, The neutral atmosphere temperature instrument, *Radio Sci.*, *8*, 287, 1973.

Spencer, N. W., L. E. Wharton, H. B. Niemann, A. E. Hedin, G. R. Carignan, and J. C. Maurer, The Dynamics Explorer wind and temperature spectrometer, *Space Sci. Instrum.*, *5*, 417, 1981.

Sperling, J. L., and S. R. Goldman, Electron collisional effects of lower hybrid drift instabilities in the ionosphere, *J. Geophys. Res.*, *85*, 3494, 1980.

Towle, D. M., VHF and UHF radar observations of equatorial *F* region ionospheric irregularities and background densities, *Radio Sci.*, *15*, 71, 1980.

Tsunoda, R. T., Time evolution and dynamics of equatorial backscatter plumes, 1, Growth phase, *J. Geophys Res.*, *86*, 139, 1981.

Tsunoda, R. T., On the generation and growth of equatorial backscatter plumes, 2, Structuring of the west walls of upwellings, *J. Geophys. Res.*, *88*, 4869, 1983.

Tsunoda, R. T., and B. R. White, On the generation and growth of equatorial backscatter plumes, 1, Wave structure in the bottomside *F* layer, *J. Geophys. Res.*, *86*, 3610, 1981.

Tsunoda, R. T., M. J. Baron, J. Owen, and D. M. Towle, ALTAIR: An incoherent scatter radar for equatorial spread *F* studies, *Radio Sci.*, *14*, 1111, 1979.

Tsunoda, R. T., R. C. Livingston, J. P. McClure, and W. B. Hanson, Equatorial plasma bubbles: Vertically elongated wedges from the bottomside *F* layer, *J. Geophys. Res.*, *87*, 9171, 1982.

Whitehead, J. D., Ionization disturbances caused by gravity waves in the presence of an electrostatic field and background wind, *J. Geophys. Res.*, *76*, 238, 1971.

Woodman, R. F., and C. LaHoz, Radar observations of *F* region equatorial irregularities, *J. Geophys. Res.*, *81*, 5447, 1976.

F. S. Johnson, R. A. Power, and S. Singh, William B. Hanson Center for Space Sciences, Physics Program, University of Texas at Dallas, Richardson, TX 75080.

(Received August 15, 1996; revised November 26, 1996; accepted December 19, 1996.)